NHTC2000-12151

HEAT TRANSFER IN A FUEL CELL ENGINE

J. Musser and C.Y. Wang
Department of Mechanical and Nuclear Engineering
Pennsylvania State University
University Park, PA 16802
Fax: (814) 863-4848   E-mail: cxw31@psu.edu

KEYWORDS: PEM, Fuel Cell Engine, Heat Generation, Current Density, System Efficiency

ABSTRACT

The polarization curve of a fuel cell stack is an effective means for comparing competing stack designs, but does not provide insight into their optimization. These enhancements can be based upon an analysis of the major contributor to the inefficiency within the fuel cell stack. This stack inefficiency is due to heat generation and is shown to be a significant source of energy losses (around 45% of the engine tested). In the process of collecting this information, the next largest contributors to inefficiencies within a fuel cell engine may also be observed. These are the requirements of pumping ambient air to the stack for reacting (around 16% of the available electrical power) and pumping coolant water through the stack to remove the excess heat (around 4% of the available electrical power). Theoretical calculations are used along with experimental measurements to determine the average heat generation rate per cell in the membranes. This heat generation is used in generating a finite volume code to predict the temperature variations across the fuel cell. After validating the code, the design decisions on the number of anode channels per plate, the materials used in the membrane and backing layers of the stack, and the supply of the coolant relative to the anode flow direction are assessed in the context of the thermal management of PEM fuel cells.

INTRODUCTION

The polarization curve of a fuel cell stack describes the performance of a stack throughout its operating range. Inefficiency within a fuel cell stack solely originates from heat generation losses due to electrochemical reactions and Joule heating. Inefficiencies in the fuel cell engine also include the parasitic losses, which are mainly to provide air for the cell and to remove the excess heat. The polarization curve for the fuel cell engine shows how these inefficiencies affect the voltage response corresponding to different loading conditions as well as provides insight into areas of improvement in stack and system designs. However, the polarization curve does not provide knowledge of the temperature distribution within a fuel cell stack resulting from heat generation.

An understanding of the thermal management within a fuel cell stack is of critical importance to the optimization of the stack design. The fuel cell stack operates more efficiently at higher operating temperatures due to increased kinetic rates at the reaction sites. However, the polymer membranes are susceptible to burning at elevated temperatures. These conflicting requirements suggest that an optimum operating temperature exists for the stack and that there is a need for a design method to show the temperature variations across the cells for various stack designs.

Calculations and experimental measurements are performed to determine the average heat generation per cell and the parasitic power requirement of the air and coolant pumps in a 1-kW fuel cell engine. This heat generation will then be used as input for a two-dimensional finite volume method (FVM) code to predict the temperature variations in the cell under various operating conditions. The code will then be used to observe the effects of design changes for improvements in the thermal management within the 1-kW stack. The efficiency of the system will also be focussed on to address the needs for improvements in other critical areas.

NOMENCLATURE

c_p	specific heat of layer material
F	Faradays constant
G	Gibbs free energy
H	enthalpy
I	current
k	thermal conductivity of layer material
P	power
$\dot{q}$	volumetric heat generation rate
S	entropy
T	absolute temperature
u	x-direction velocity within layer material
V	voltage or volume
v	y-direction velocity within layer material
x	direction along layers
y	direction across layers
z	number of electrons per mole of fuel

Greek Symbols

ρ	density of layer material
μ	viscosity of layer material
Δ	change in property
Φ	viscous heat generation within layer material

Subscripts

total	total
heat	thermal
electrical	electrical
cell	cell
membrane	membrane

ANALYSIS

Determination of Heat Generation Rate

The heat generation rate per cell in the stack, as posed by Thomas and Zalbowitz (1999), is based on the theoretical and experimental cell voltage and current. The equation is an energy rate balance between the cell products and reactants, the heat generation, and the measured electrical power.

$$P_{total} = P_{heat} + P_{electrical} \qquad (1)$$

$$\left(V_{ideal} * I_{cell}\right) = P_{heat} + \left(V_{cell} * I_{cell}\right) \qquad (2)$$

$$P_{heat} = \left(V_{ideal} - V_{cell}\right) * I_{cell} \qquad (3)$$

Thomas and Zalbowitz (1999) also presented the theoretical calculations to predict the maximum theoretical cell voltage (V_{ideal}) in a fuel cell system from fundamental thermodynamics. The enthalpy of the products entering the fuel cell at a given temperature and pressure can be broken up into the Gibbs free energy available for useful work and the losses experienced at the surface due to entropy changes.

$$\Delta H = \Delta G + T\Delta S \qquad (4)$$

The maximum cell voltage (V_{ideal}) attainable from this available energy (ΔG) can then be calculated using Faradays constant and the number of electrons exchanged (z) in the cell reaction.

$$V_{ideal} = -\frac{\Delta G}{zF} = \frac{T\Delta S - \Delta H}{zF} \qquad (5)$$

Experimental

The measured cell voltage (V_{cell}) is found from the system polarization curve, which is obtained through experimental measurements on a 1-kW fuel cell engine operating throughout the range of interest. The stack consists of a repeated pattern of electrode and coolant plates, membranes, and backing layers (Figure 1).
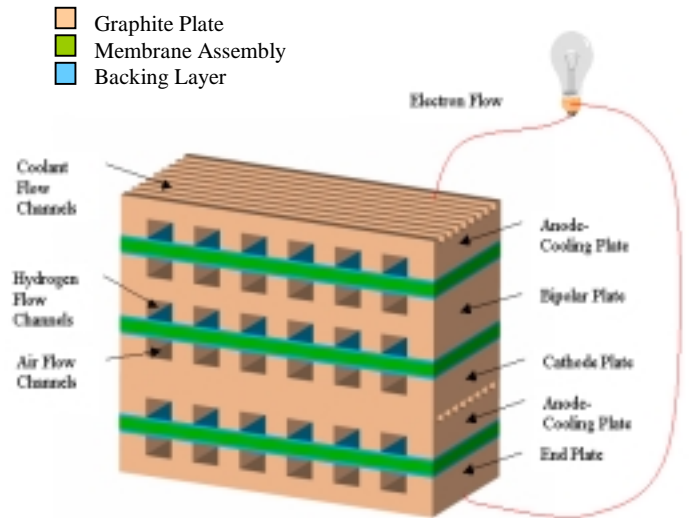

Figure 1: Schematic of the Fuel Cell Stack Layering

Each of the twenty membranes has an effective activation area of 240 cm^2, which is debatable if the backing layers and graphite channels are not effective at evenly distributing the reactants. The coolant and electrode flow channels are machined from graphite plates (Figure 2). The anodes have three sets of channels where hydrogen is delivered from the inlet manifold. This hydrogen is consumed along the length of the channel, until there is no hydrogen left for reacting. In this stack there are a total of ten anode-coolant plates each consisting of thirty-two coolant flow channels through which deionized water is pumped to remove the heat produced by the cell reactions.
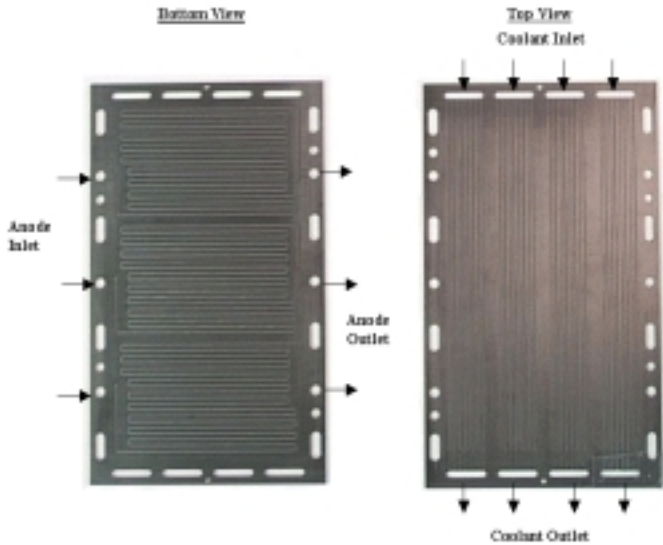
2

Figure 2: Schematic of an Anode-Cooling Plate

The 1-kW engine consists of the stack, air pump, heat exchanger, coolant pump, load, and controller (Figure 3).
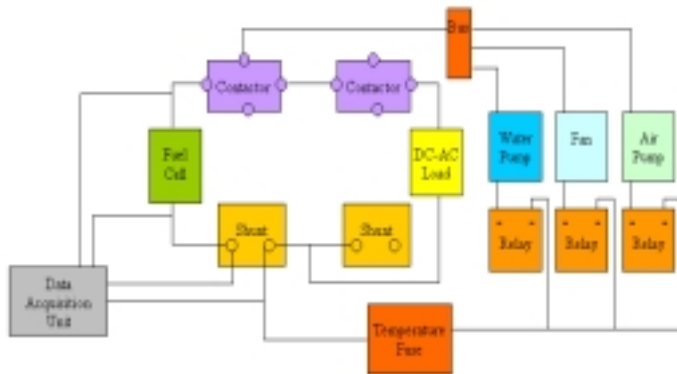

Figure 3: Schematic of the Experimental Fuel Cell Stack Layout

The parasitic systems (air pump, heat exchanger fan, and coolant pump) are attached in parallel and controlled using pulse-width modulation (PWM). The parameters measured by the data acquisition system are the stack current and voltage and the coolant inlet and outlet temperatures. The experimental cell voltage (V_{cell}) for the polarization curve is then calculated by dividing the measured stack voltage by the number of cells in the stack. The current and voltage readings for the heat exchanger fan and coolant pump are also recorded for each measurement. The load for the electrochemical experiment is the Arbin testing system, which is used to control the amount of current drawn over the desired duty schedule. For the heat transfer experiment, the load is simply

to run the lights for the laboratory through the use of a DC to AC converter.

Heat Transfer Analysis

The heat generation calculations and measurements are then used in a finite volume method (FVM) code to predict the temperature variations within the fuel cell stack. In the finite volume method, as presented by Patankar (1980), the domain is split up into a number of control volumes each containing a grid point (node). The sides of the control volumes are then the shared interfaces between neighboring nodes. The differential equations governing the system are then discretized and integrated over each control volume to iteratively solve for the desirable field.

The geometry for the model design (Figure 4) is based on the stack design of the 1-kW engine used in the experimental measurements.
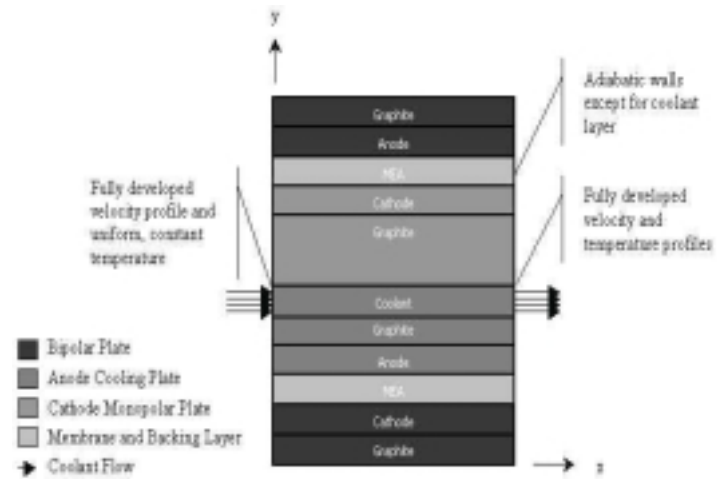

Figure 4: Schematic of FVM Model

The coolant plates are spaced within the stack such that a temperature gradient does not exist across the bipolar plates for heat transfer to occur: thus, adiabatic walls are assumed at both the top and bottom of the model. Since the ends of the model are within the fuel cell stack (not exposed to the ambient conditions) and the model is also slender (7.58 in. long and 0.28 in. thick), adiabatic walls were also chosen for the left and right walls above and below the coolant channel. The inlet temperature of the coolant is assigned to be the inlet temperature of the stack used in the experiment, and the length of the channel is sufficient for a fully developed temperature profile to be assumed at the outlet. The average velocity of the coolant flow within the channel is found by dividing the pump flow rate by the number of channels within the stack. From this and the geometry of the channel, the coolant flow in the model is found to be laminar (Re_D=410<<2300) and is assumed to have a fully developed velocity profile (1.1cm

3   Copyright © 2000 by ASME

entrance length<<19.3cm model length) everywhere within the channel (Incropera and DeWitt, 1996). Due to the simple flow pattern within the coolant channel, the nodes are assigned a velocity based on the pipe flow rather than using the FVM code to solve for the velocity profile. Finally, a simplifying assumption, that may need to be revisited for a more complete analysis, is that the interfacial resistance due to imperfect surface contact between the stacked layers is insignificant for the calculation of the temperature profile within the model.

The governing equations describing the steady state heat transfer within the fuel cell are based on an energy balance within a control volume (Incropera and DeWitt, 1996). The system is truly a three-dimensional problem, but for simplification, the cathode air flow is assumed to remove a negligible amount of heat from the stack. Therefore, the two-dimensional, steady state heat transfer equation is:

$$\rho c_p \left(u \frac{\partial T}{\partial x} + v \frac{\partial T}{\partial y} \right) = \frac{\partial}{\partial x} \left(k \frac{\partial T}{\partial x} \right) + \frac{\partial}{\partial y} \left(k \frac{\partial T}{\partial y} \right) + \mu \Phi + \dot{q} \qquad (6)$$

Since the coolant flow is laminar, the heat dissipation due to the conversion of kinetic to thermal energy by the viscous flow of the coolant is assumed negligible. The coolant velocity has flow only in the x-direction. The thermal conductivity is assumed to be constant with respect to spatial orientation. Finally, the heat generation rate is found by dividing the average heat generation rate by the volume of an individual membrane. However, this heat generation rate is dependent on x-location and is assumed to vary linearly as the supply of hydrogen is consumed from the anode inlet (two times P_{heat}) to outlet (zero), as shown in Figure 5, for the model under consideration.
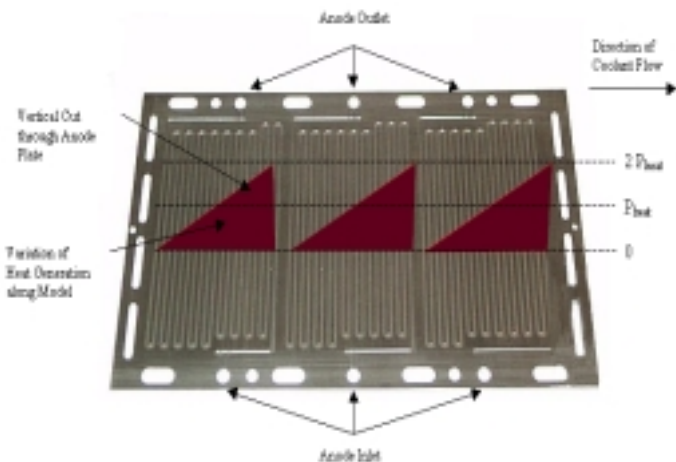

Figure 5: Variation of Heat Generation along MEA for Model

Under these assumptions, Eq. (6) becomes

$$\rho c_p u \frac{\partial T}{\partial x} = k \frac{\partial^2 T}{\partial x^2} + k \frac{\partial^2 T}{\partial y^2} + \frac{P_{heat}}{V_{membrane}} \qquad (7)$$

for the coolant channel. For all the layers except the coolant channel, the velocity is also zero, and the governing equation for these layers reduces to

$$0 = k \frac{\partial^2 T}{\partial x^2} + k \frac{\partial^2 T}{\partial y^2} + \frac{P_{heat}}{V_{membrane}} \qquad (8)$$

The thermophysical properties selected for use in solving the governing equations were either that of the materials used in the 1-kW engine or that of a similar material (Table 1).

Layering Material	Thermal Conductivity (W/m•K)	Specific Heat (J/kg•K)	Density (kg/m³)
Graphite	85.5	691	2120
PEM	0.2	1500	1100
Backing	10	709	2000
Coolant	0.7	4188	983
Anode	42.8	7500	1060
Cathode	42.7	849	1060

Table 1: Thermophysical properties of materials in fuel cell stack

The thermal conductivity, specific heat, and density of the graphite used in the plates were provided by the manufacturer (H-Power, 1999). The properties of the membranes and backing layers are selected to be those of a polymer and of plain carbon (Callister, 1997). The properties of the coolant are assumed to be that of regular water (White, 1994). The properties of the anode and the cathode layers are an average of those used for the graphite layers and either air or hydrogen (Incropera and DeWitt, 1996).

RESULTS AND DISCUSSION

Electrochemical Results

A polarization curve was generated for the 1-kW engine (Figure 6), which is to be used for selecting the stack voltage and corresponding current values for the FVM code thermal analysis. It is also a beneficial tool to show the system losses by the parasitic devices.
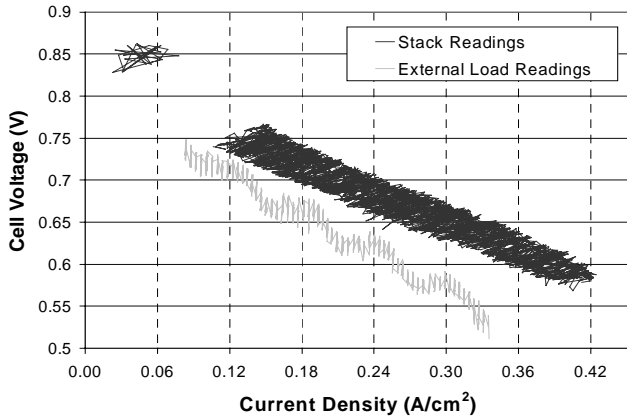
Figure 6: Polarization Curve for 1-kW Fuel Cell Engine

For the electrochemical results, data was collected using the Arbin testing system as a load rather than the laboratory lights. This allowed for better control of drawn current, but only permitted data collection below a stack voltage of 15 V. The scattering of data at a cell voltage of 0.85 V was collected after the external load was removed. However, the parasitic devices (air pump, coolant pump, and heat exchanger fan) were still drawing current from the stack. As the load current was increased, the cell voltage drop went through cycles that corresponded to the settings of the pulse width modulation of the air pump (dashed vertical lines).

The air pump is the major contributor to parasitic losses within the engine, requiring 171 W of the available 1088 W from the stack (16%). By increasing the number of bins and decreasing their width around the desired operating range, this inefficiency can be decreased as can be seen by the difference between the stack power and corresponding available load power in Figure 7.
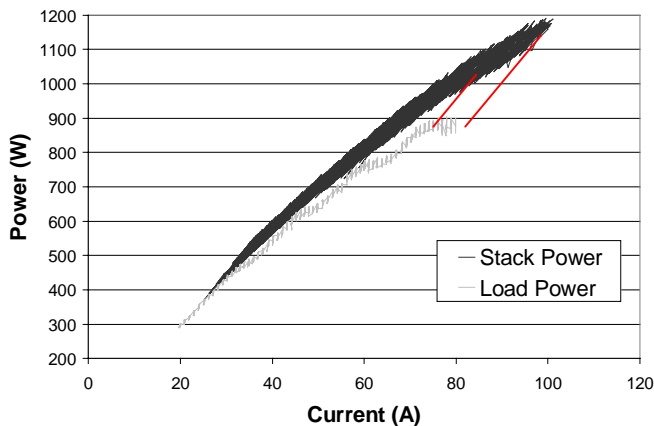
For a load power of 875 W, the cell voltage decreases by the same amount that the current increase leading to a stack power that can vary from 1050 to 1150 W. This suggests that there is a 100 W loss to the system by using the wide bins in the PWM control. However, if only a limited number of bins are available by the controller, then an efficiency sacrifice is required to increase the range of operation of the fuel cell engine.

For controller simplicity, the coolant pump is not operated using pulse width modulation. Rather, it runs at a constant rate of 3.5 LPM and consumes 41 W. At a stack power of 1088 W, 4% of the total available electrical power is consumed to operate the coolant pump.

Heat Transfer Results

The heat generation within the membrane layer is calculated based on the theoretical calculations and the experimental measurements. The results of the theoretical calculations are that the theoretical maximum cell voltage is 1.20 V for an air/hydrogen system operating at 1 atmosphere and 45°C. The experimentally measured average cell voltage is 0.70 V at 47.5 A and 0.65 V at 68.9 A. These provide for an average heat generation of 479.8 and 764.8 W, for the 1-kW stack operating at 660.3 and 888.8 W, respectively. The result is that 42 and 46% of the energy provided to the fuel cell is dissipated due to the combination of the resistance of ion conductivity through the membrane and entropy changes at the electrodes.

With the heat generation determined, a comparison between the predicted and the measured exit temperatures may be performed to validate the assumptions of the FVM model. Figure 8 shows the outlet temperatures for both the FVM model and the experimental measurements as a function of the coolant flow rate. The FVM code slightly under-predicts the coolant outlet temperatures compared to the measured
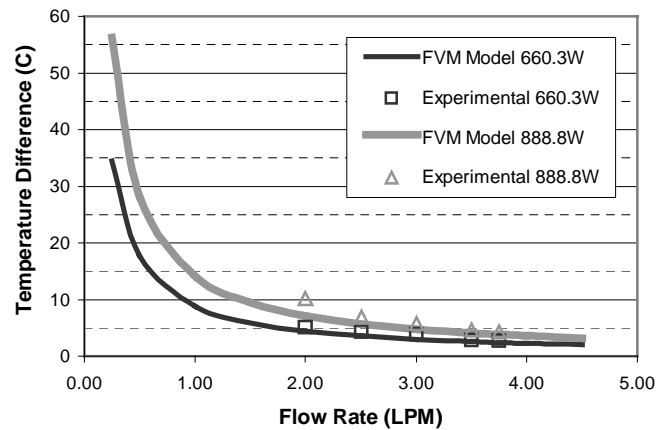

Figure 7: Stack and External Load Power as Functions of Current

Figure 8: Experimental and Calculated Coolant Outlet Temperatures as Functions of Coolant Flow Rate

temperature for the given loading condition. Therefore, the assumption that the air flowing through the cathode does not remove a significant amount of heat from the stack appears valid since this would have the code over-predicting the coolant outlet temperature as opposed to the observed under-prediction.

Now that the FVM model has been validated, it may then be used to determine the temperature variations occurring within the fuel cell stack under various conditions. Figure 9 shows the code predictions for the coolant outlet and maximum cell temperatures as functions of coolant flow rate into the stack.
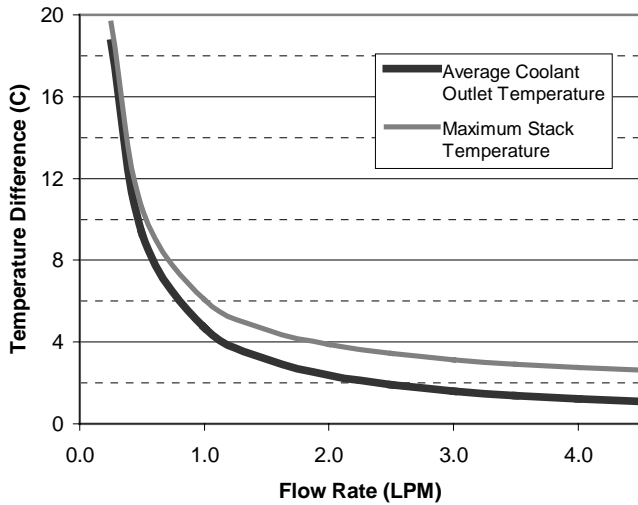
Figure 9: Coolant Outlet Temperature and Maximum Cell Temperature as Functions of Coolant Flow Rate

The outlet temperature varies insignificantly with increased coolant flow for rates greater than 2.5 LPM. The maximum temperature within the stack is approximately 1.5 degrees higher than the coolant outlet temperature for all flow rates greater than 1 LPM. However, if the interfacial resistance between the stack layers shows to be significant, then the maximum temperatures would increase from those recorded for all flow rates.

In addition, the power required to pump the coolant through the stack was also recorded for the flow rates measured (Figure 10). The results show that for flow rates above 2.50 LPM the power requirements become substantially higher than the thermal benefit obtained from the higher flow rate.

The effects of various stack design changes are also observed by using the validated FVM code. The first design change is to see the effect on internal temperature to both an increase and a decrease in the number of sets of anode flow channels (Figure 11).
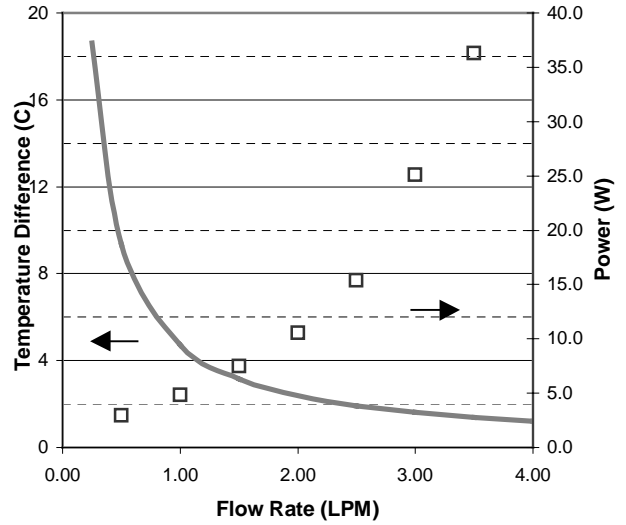
Figure 10: Temperature Rise along Stack and Parasitic Power Requirement of Coolant Pump as Functions of Coolant Flow Rate
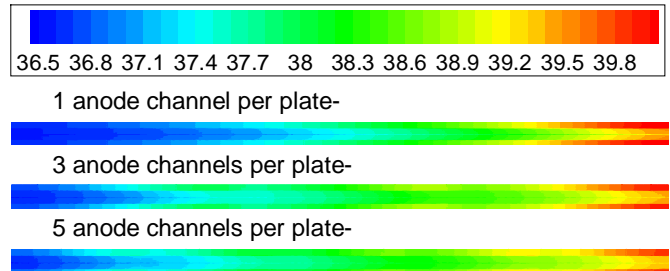
Figure 11: Temperature Contours for Various Numbers of Anode Channels per Plate

Since the current density was assumed to linearly decrease from anode inlet to outlet, more anode channels per plate results in a more uniform temperature along the membranes. However, the change is only slight and may introduce problems in practice when considering the manifolds for delivering the coolant, air, and hydrogen into the stack.

The next design consideration was to look at the dependence of the temperature within the stack on the material properties of the membrane and backing layers. The properties for these layers are being revisited since the values selected for the code were not that of the exact materials used in the stack. The membrane and backing layers are solid layers and thus are not governed by the specific heat and density (Eq. 8). For both the much higher (10 times) and much lower (1/10 times) property values of thermal conductivity, the FVM code predicts the same coolant outlet temperature. However, the maximum stack temperature for the much higher case is 0.46 degrees cooler. While for the much lower case, the maximum stack

6   Copyright © 2000 by ASME

temperature is 3.98 degrees higher. These phenomena can be explained as the heat being trapped within the bipolar plate by the materials with a low thermal conductivity and allowed to move more freely through the materials with a high thermal conductivity. A similar phenomena may be observed if the interfacial resistance is found to be significant.

The last observation was to see the effect of simply reversing the direction of the hydrogen flow within the anode. Figure 12 shows the contours of the temperature within the stack for this case.
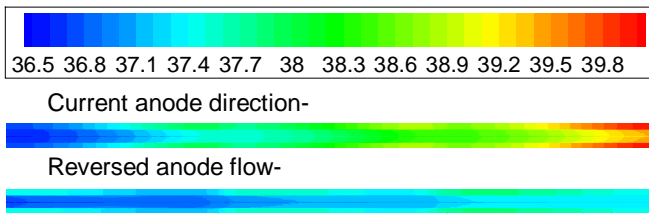

Figure 12: Temperature Contours for Reversed Coolant Flow

By reversing the direction of the hydrogen, the cooler water at the coolant inlet has a better ability to reduce the higher temperatures experienced at the anode inlet. There is also no heat generation at the anode outlet near the coolant outlet were the water temperature is highest. The result is a more uniform temperature along the membrane, which can provide for more efficient control of the stack internal temperature.

CONCLUSION

The major contributors to inefficiencies in a fuel cell engine were examined. The heat generation within the stack was shown to decrease the performance by around 45% of the energy from the reactants. The parasitic load of running an air pump to provide for the cathode was measured to be around 16% of the available electrical power. While operating the coolant pump required another 4% of the available electrical power. These two contributions result in a 58% system efficiency loss. These are, however, engineering possibilities and not thermodynamic limits as experienced in heat engines.

FVM has been shown to be an effective tool to safely determine the operating temperature within a fuel cell engine. The ability of FVM for fuel cell stack designers is also observed due to the flexibility and relative ease of design modifications as compared to prototyping first round concepts. Stack parameters (cell voltage and current) may be selected from a polarization curve and then introduced into a FVM model to evaluate the thermal management within the stack. Various coolant flow rates and designs may also be examined without concern for burning the membranes. Increasing the number of anodes per plate was observed to provide a slightly

more uniform stack temperature since it provided for a more uniform distribution of the hydrogen. Designing the coolant flow to be introduced where the heat generation is a maximum provided a much more uniform and lower stack temperature.

The effect of the interfacial contact resistance on the maximum temperature within the stack will be investigated in future work. Experimental work will be performed to confirm the code predictions. The temperature dependence on this resistance will be determined to aid in future stack designs.

The linear simplification for current density will also be examined with modifications to the FVM code. This will be done by examining the amount of hydrogen available along the length of the channel for reacting.

Finally, the effects of reversing the direction of the coolant flow with respect to the anode flow will also be experimentally studied. Preliminary work with the FVM code shows a more uniform temperature along the membrane and a lower overall coolant temperature. The results, if confirmed, would allow for a simple redesign of the system to provide for more efficient control of the stack temperature. A lower coolant temperature also translates into less heat for the heat exchanger to remove.

REFERENCES

Callister, W. (1997). "Materials Science and Engineering," John Wiley and Sons, New York, pp. 775,776,792-796.

H-Power Corporation (1999). Private communications.

Incropera, F. and DeWitt, D. (1996). "Fundamentals of Heat and Mass Transfer," John Wiley and Sons, New York, pp. 303, 421,449,846.

Patankar, S. (1980). "Numerical heat Transfer and Fluid Flow," Taylor and Francis.

Thomas, S. and Zalbowitz, M. (1999). "Fuel Cells – Green Power," Los Alamos National Laboratory.